Electronic Supplementary Material (ESI) for Journal of Materials Chemistry C.


# Lightweight, Superelastic, and Temperature-Resistant rGO/Polysulfoneamide-Based Nanofiber Composite Aerogel for Wearable Piezoresistive Sensor

*Ziwen Wang,[a] Zhen Qin,[a] Biao Zhao,[a] Han Zhu*[b] and Kai Pan*[a]*

a State Key Laboratory of Organic-Inorganic Composites, Beijing Key Laboratory of Advanced Functional Polymer Composites, College of Materials Science and Engineering, Beijing University of Chemical Technology, Beijing 100029, China.

* E-mail: pankai@mail.buct.edu.cn

b College of Materials Science and Engineering, Beijing University of Chemical Technology, Beijing, China

* E-mail: zhuhan@mail.buct.edu.cn

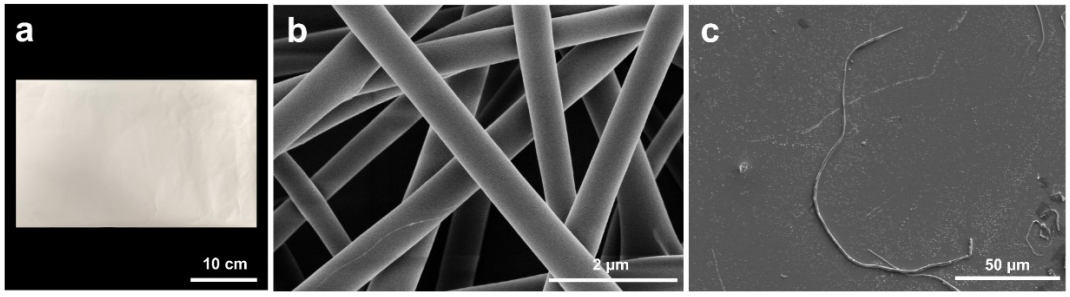


**Fig. S1 (**a) The picture of PSAN nanofiber film, (b) the SEM image of PSAN nanofiber film, (c) the SEM image of homogenized PSAN nanofiber.

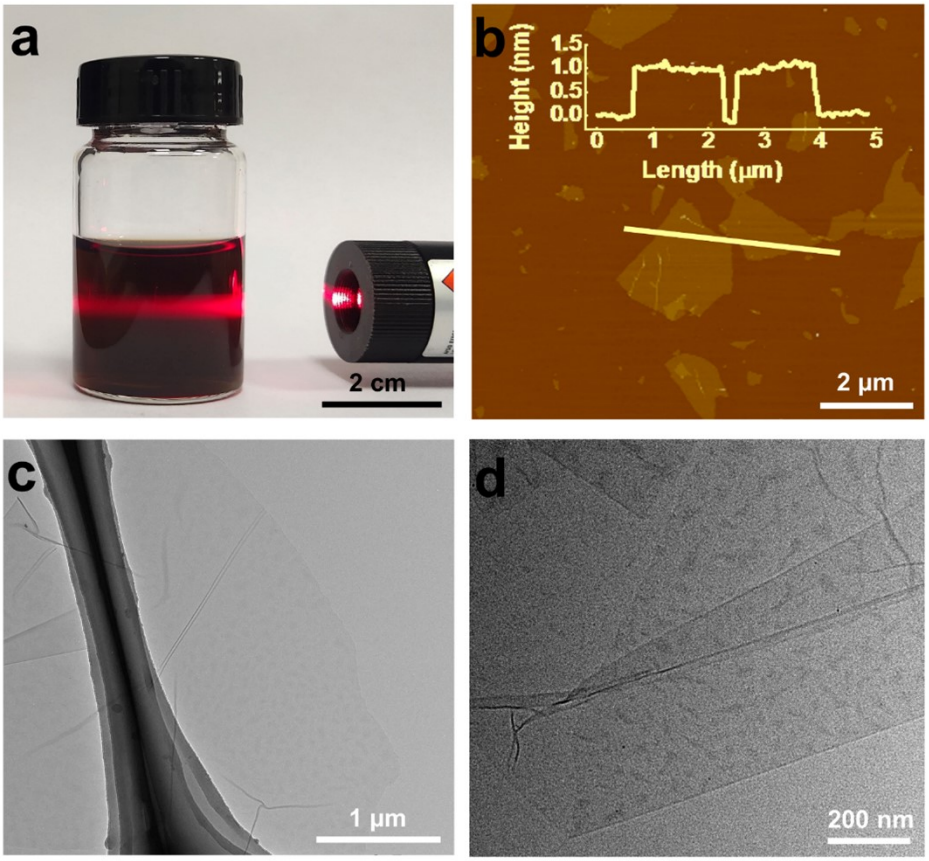


**Fig. S2 (**a) The digital picture of GO dispersion, (b) the AFM image of GO nanosheets, (c,d) the TEM images of GO nanosheets.

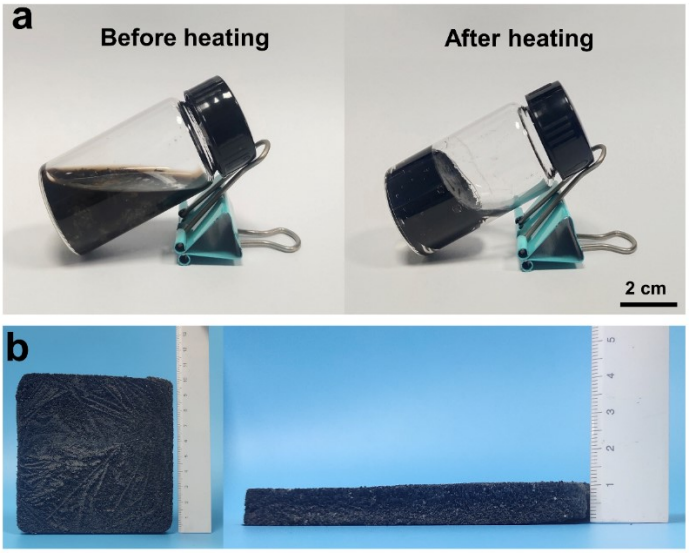


**Fig. S3** (a) The mixed solution of GO dispersion and PSAN nanofibers formed hydrogel after heating, (b) GA can be fabricated into large size.

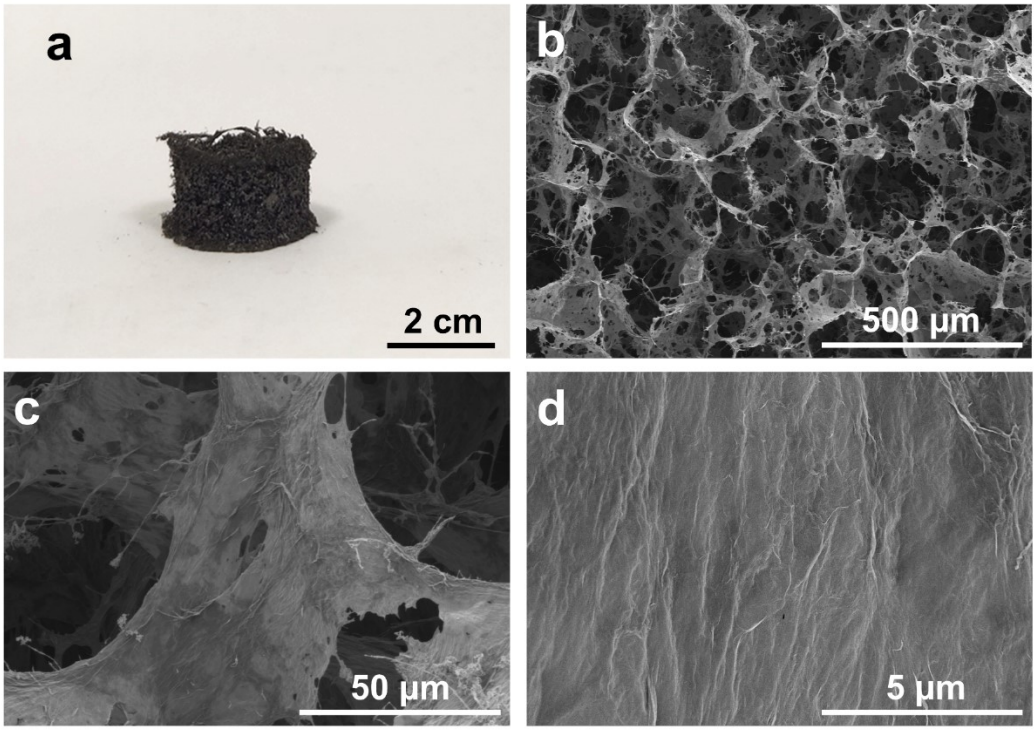


**Fig. S4 (**a) Digital picture of the prepared rGO aerogel, SEM images inside rGO aerogel with (b) interconnected porous structure and (c,d) smooth pore wall structure.

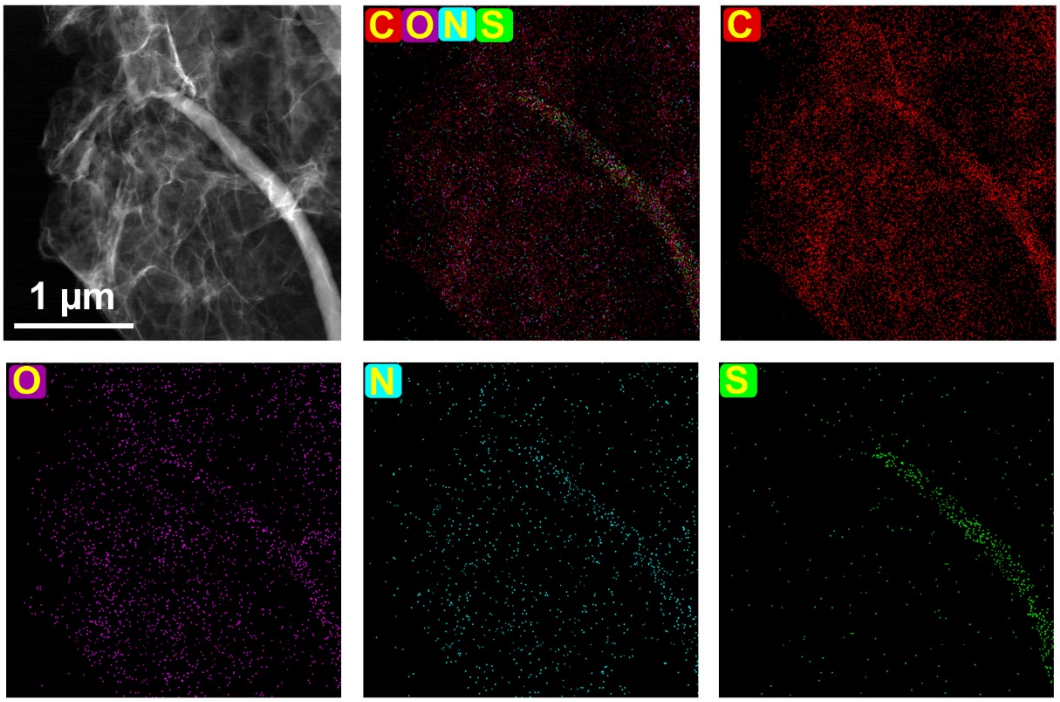


**Fig. S5** Elements distribution on the pore wall of GA-1.

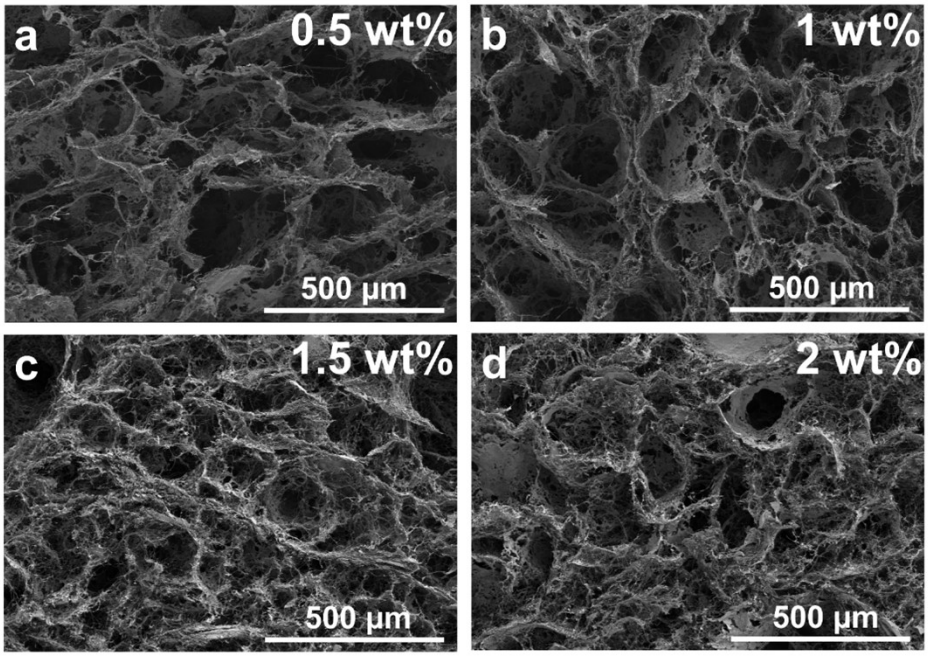


**Fig. S6** Pore structures of GA with PSAN nanofiber contents of (a) 0.5 wt%, (b) 1 wt%, (c) 1.5 wt%, and (d) 2 wt%, respectively.

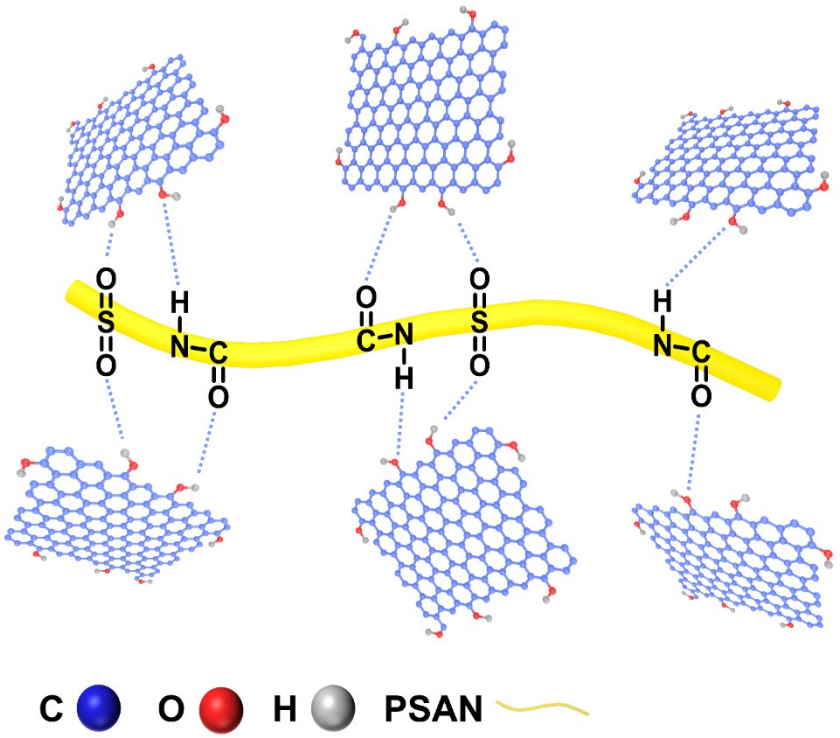


**Fig. S7** Schematic illustration of hydrogen bonds formation between rGO nanosheets and PSAN nanofibers.

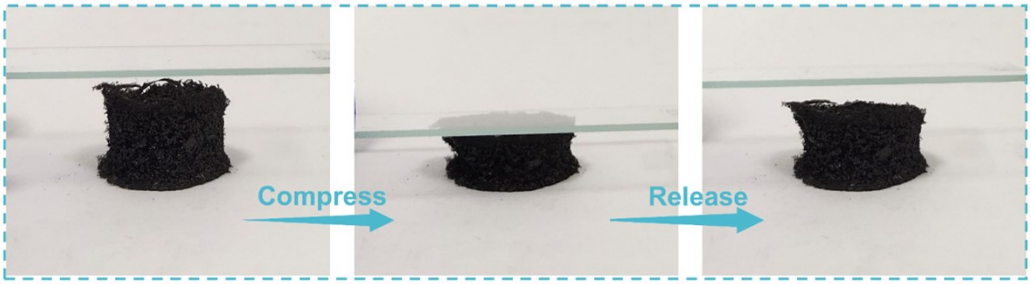


**Fig. S8** Compression and recovery process of rGO aerogel.

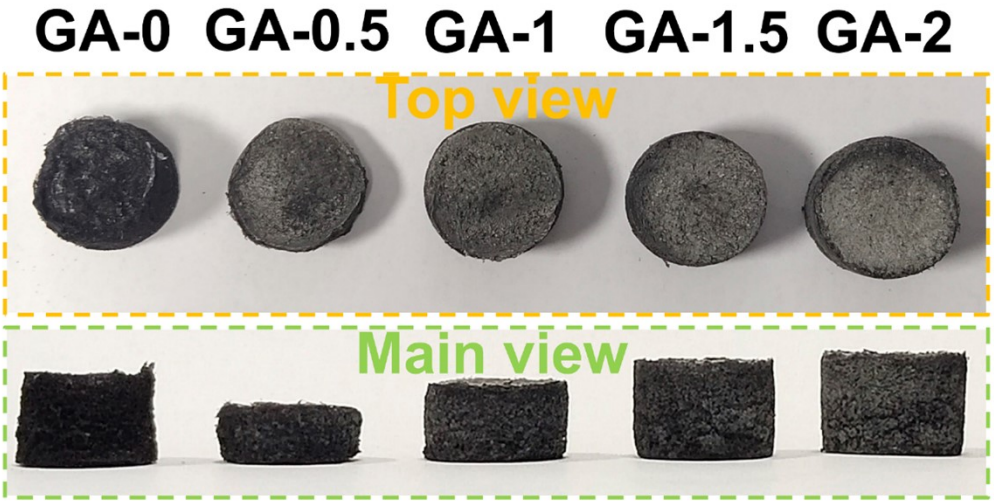


**Fig. S9** Top and main views of rGO aerogel and GA with different PSAN nanofiber contents.

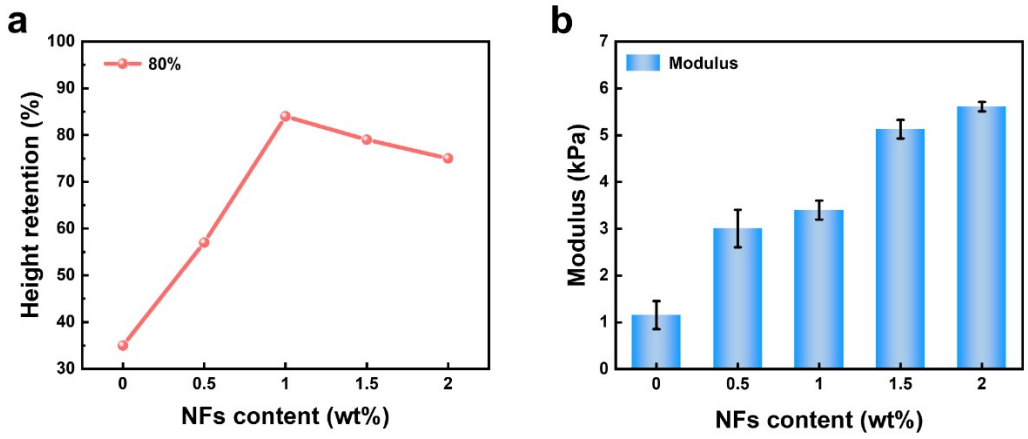


**Fig. S10** (a) The height retention of GA with different PSAN nanofiber contents under 80% strain, (b) the compression modulus of GA with different PSAN nanofiber contents.

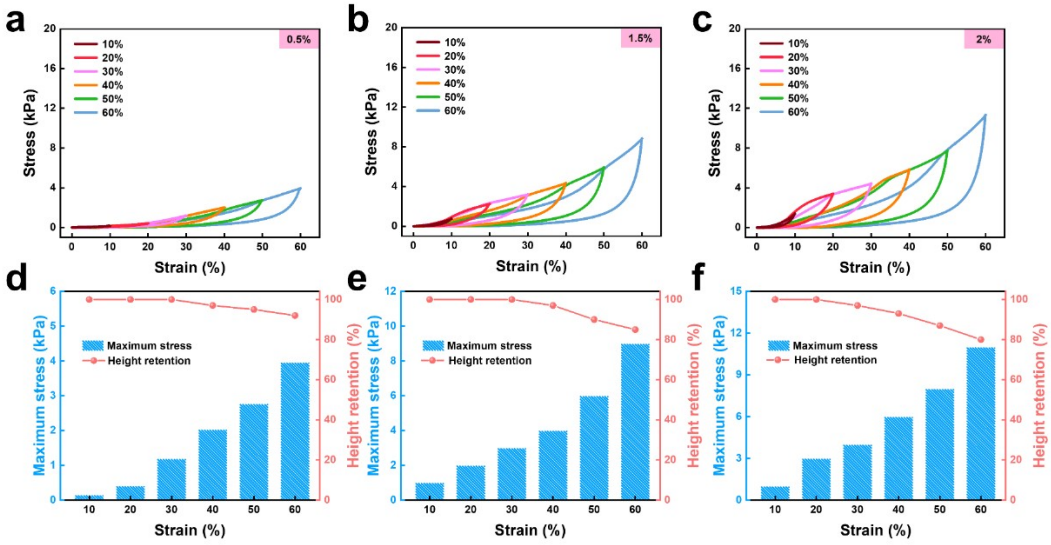


**Fig. S11** (a-c) Stress-strain curves and (d-f) height retention and maximum strength of GA with PSAN nanofiber content of 0.5 wt%, 1.5 wt% and 2 wt% under 10-60% strain, respectively.

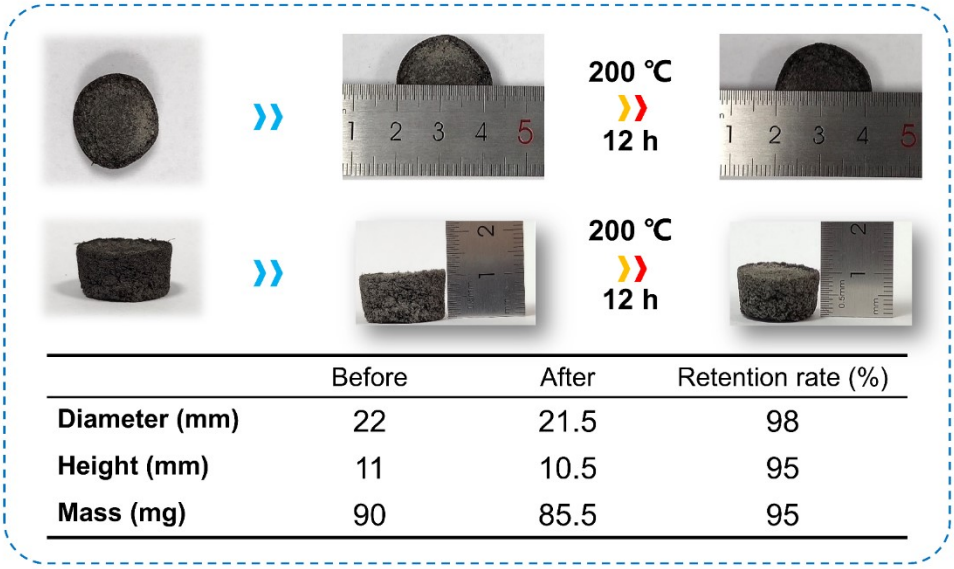


| | Before | After | Retention rate (%) |
|---|---|---|---|
| **Diameter (mm)** | 22 | 21.5 | 98 |
| **Height (mm)** | 11 | 10.5 | 95 |
| **Mass (mg)** | 90 | 85.5 | 95 |

**Fig. S12** Changes in shape, size and mass of GA-1 after being heated at 200 °C for 12 h.

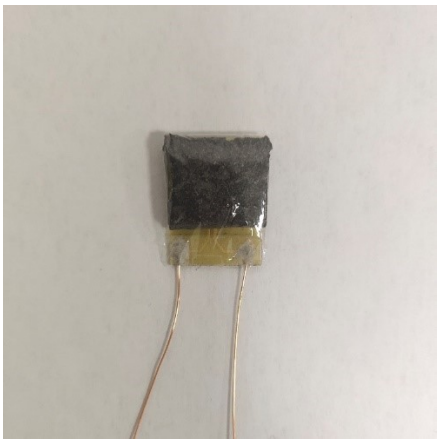

**Fig. S13** Picture of the GA-based flexible piezoresistive sensor.

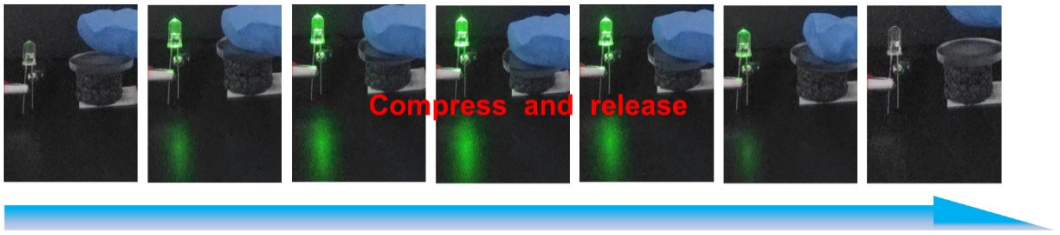


**Fig. S14** The brightness of LED varies with GA-1 during compression and recovery process.

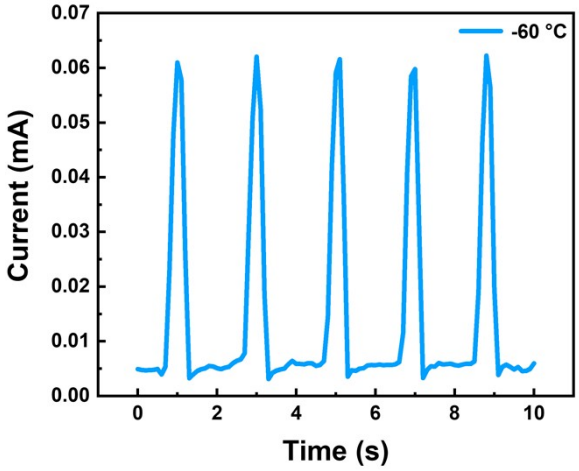


**Fig. S15** The piezoresistive sensing performance of GA-1-based piezoresistive sensor at -60 °C.

**Table S1** Performance comparison of flexible pressure sensors based on rGO aerogel.

| Materials | Pressure range | Sensitivity | Compression strength | Durability | Response time | Recovery time | Reference |
|---|---|---|---|---|---|---|---|
| rGO/ANF/PANI<br>T | ~0.7 kPa<br>0.7~7 kPa | 1.73 $kPa^{-1}$<br>0.3 $kPa^{-1}$ | 3 kPa (45%) | 3000 | 240 ms<br>(10%) | 140 ms<br>(10%) | [1] |
| CNF/CNT/rGO | ~0.21 kPa | 5.61 $kPa^{-1}$ | 1.2 kPa<br>(80%) | 2000 | - | - | [2] |
| BC/rGO | ~2.54 kPa<br>2.54~12 kPa | 13.89 $kPa^{-1}$<br>2.71 $kPa^{-1}$ | 52 kPa (80%) | 1000 | 120 ms | 540 ms | [3] |
| CNT/rGO | ~0.5 kPa<br>0.5~3.5 kPa | 7 $kPa^{-1}$<br>11.8 $kPa^{-1}$ | 11.5 kPa<br>(60%) | 2000 | 317 ms | 303 ms | [4] |
| PAN/rGO | ~14 kPa | 28.62 $kPa^{-1}$ | 43.54 kPa<br>(80%) | 2600 | 305 ms<br>(2634 Pa) | 165 ms<br>(2634 Pa) | [5] |
| MXene/rGO | ~3.3 kPa<br>3.3~6.4 kPa<br>6.4~10.1 kPa | 61 $kPa^{-1}$<br>334 $kPa^{-1}$<br>609 $kPa^{-1}$ | 11.5 kPa<br>(80%) | 17000 | 232 ms | 225 ms | [6] |
| rGO | ~3.9 kPa<br>3.9~13.56 kPa | 9.13 $kPa^{-1}$<br>7.29 $kPa^{-1}$ | 6 kPa (80 %) | 10000 | 0.35 s<br>(1.43kPa) | 0.39 s<br>(1.43kPa) | [7] |
| PI/rGO | ~0.52 kPa<br>20~59 kPa | 1.33 $kPa^{-1}$<br>0.002 $kPa^{-1}$ | 60 kPa<br>(80%) | 1000 | 60 ms<br>(0.5%) | 70 ms<br>(0.5%) | [8] |
| PPy/rGO | ~1 kPa<br>1~9 kPa | 0.9 $kPa^{-1}$<br>0.0122 $kPa^{-1}$ | - | 10000 | 165 ms | 132 ms | [9] |
| MXene/rGO | ~0.2 kPa<br>0.2~2 kPa | 6.22 $kPa^{-1}$<br>2.53 $kPa^{-1}$ | 4.5 kPa (90%) | 1250 | 8 ms | 50 ms | [10] |
| GA-1 | ~24.97 kPa | 32.85 $kPa^{-1}$ | 26.07 kPa<br>(80%) | 3500 | 300 ms<br>(20%) | 200 ms<br>(20%) | This Work |

## Reference:


1. Y. B. Zou, Z. Y. Chen, X. Guo, Z. Y. Peng, C. Y. Yu and W. B. Zhong, *ACS Appl. Mater. Interfaces*, 2022, **14**, 17858-17868.
2. H. Y. Liu, T. Xu, C. Y. Cai, K. Liu, W. Liu, M. Zhang, H. S. Du, C. L. Si and K. Zhang, *Adv. Funct. Mater*., 2022, **32**, 2113082.
3. S. Wei, X. Y. Qiu, J. Q. An, Z. M. Chen and X. X. Zhang, *Compos. Sci. Technol.*, 2021, **207**, 108730.
4. H. Zhu, S. P. Dai, X. S. Zhou, X. Dong, Y. Y. Jiang, Y. W. Chen, N. Y. Yuan and J. N. Ding, *J. Compos. Mater.*, 2021, **55**, 3661-3669.
5. X. Y. Cao, J. Zhang, S. W. Chen, R. J. Varley and K. Pan, *Adv. Funct. Mater.*, 2020, **30**, 2003618.
6. M. Zhu, Y. Yue, Y. F. Cheng, Y. Zhang, J. Su, F. Long, X. L. Jiang, Y. Ma and Y. H. Gao, *Adv. Electron. Mater.*, 2019, **6**, 1901064.
7. J. K. Huang, J. B. Zeng, B. Q. Liang, J. W. Wu, T. G. Li, Q. Li, F. Feng, Q. W. Feng, M. J. Rood and Z. F. Yan, *ACS Appl. Mater. Interfaces*, 2020, **12**, 16822-16830.
8. Q. Xu, X. H. Chang, Z. D. Zhu, L. Xu, X. C. Chen, L. B. Luo, X. Y. Liu and J. Q. Qin, *RSC Adv.*, 2021, **11**, 11760-11770.
9. H. Wei, A. Li, D. Kong, Z. Li, D. Cui, T. Li, B. Dong and Z. Guo, *Adv. Compos. Hybrid Mater.*, 2021, **4**, 86-95.
10. L. Liu, J. Zhang, G. Shi, H. Zhang, B. Wang and L. Zhong, *J. Mater. Sci.*, 2022, **57**, 11202-11214.